frontiers | Frontiers in Forests and Global Change

TYPE Original Research
PUBLISHED 06 October 2023
DOI 10.3389/ffgc.2023.1166349

OPEN ACCESS

EDITED BY
Thomas J. Dean,
Louisiana State University, United States

REVIEWED BY
Pinliang Dong,
University of North Texas, United States
Cory Garms,
Spectral Sciences, United States

*CORRESPONDENCE
Jiayuan Lin
joeylin@swu.edu.cn

RECEIVED 25 May 2023
ACCEPTED 04 September 2023
PUBLISHED 06 October 2023

CITATION
Lin J, Chen D, Yang S and Liao X (2023) Precise aboveground biomass estimation of plantation forest trees using the novel allometric model and UAV-borne LiDAR.
Front. For. Glob. Change 6:1166349.
doi: 10.3389/ffgc.2023.1166349

Precise aboveground biomass estimation of plantation forest trees using the novel allometric model and UAV-borne LiDAR

Jiayuan Lin[1]*, Decao Chen[1], Shuai Yang[1] and Xiaohan Liao[2]

[1]Chongqing Jinfo Mountain Karst Ecosystem National Observation and Research Station, School of Geographical Sciences, Southwest University, Chongqing, China, [2]Institute of Geographic Sciences and Natural Resources Research, Chinese Academy of Sciences, Beijing, China

Introduction: Plantation forest is an important component of global forest resources. The accurate estimation of tree aboveground biomass (AGB) in plantation forest is of great significance for evaluating the carbon sequestration capacity. In recent years, UAV-borne LiDAR has been increasingly applied to forest survey, but the traditional allometric model for AGB estimation cannot be directly used without the diameter at breast height (DBH) of individual trees. Therefore, it is practicable to construct a novel allometric model incorporating the crown structure parameters, which can be precisely extracted from UAV LiDAR data. Additionally, the reduction effect of adjacent trees on crown area (A_C) should be taken into account.

Methods: In this study, we proposed an allometric model depending on the predictor variables of A_C and trunk height (H). The UAV-borne LiDAR was utilized to scan the sample plot of dawn redwood (DR) trees in the test site. The raw point cloud was first normalized and segmented into individual trees, whose A_Cs and Hs were sequentially extracted. To mitigate the effects of adjacent trees, the initial A_Cs were corrected to refer to the potential maximum A_Cs under undisturbed growth conditions. Finally, the corrected A_Cs (A_{CC}) and Hs were input into the constructed allometric model to achieve the AGBs of DR trees.

Results and discussion: According to accuracy assessment, coefficient of determination (R^2) and root mean square error (RMSE) of extracted Hs were 0.9688 and 0.51 m; R^2 and RMSE of calculated AGBs were 0.9432 and 10.91 kg. The unrestricted growth parts of the tree crowns at the edge of a plantation forest could be used to derive the potential maximum A_C. Compared with the allometric models for AGB estimation relying only on trunk H or on initial A_C and H, the novel allometric model demonstrated superior performance in estimating the AGBs of trees in a plantation forest.

KEYWORDS

plantation forest, aboveground biomass (AGB), UAV-borne LiDAR, allometric model, trunk height, crown area

1. Introduction

Plantation forestry is gradually becoming a significant component of global forest resources (FAO, 2020) and is playing an increasingly crucial role in the global carbon cycle (Fang et al., 2001; Lal, 2005; Chen et al., 2011; Lun et al., 2018; Diao et al., 2022). More importantly, the contribution of plantation forest is expected to surpass that of natural forest in carbon neutralization (Justine et al., 2015; Chen et al., 2022). As the key indicator,

the aboveground biomass (AGB) of a forest is vital for quantitatively estimating its carbon sequestration (Dubayah et al., 2010; Chen et al., 2015; Li et al., 2015; Dube and Mutanga, 2016; Lu et al., 2017; Su et al., 2020). Furthermore, the tree AGB is the primary component of the total biomass of a plantation forest (Ming et al., 2012; Yu et al., 2013; Zheng et al., 2014; Li, 2019; Guo et al., 2022). Therefore, the accurate AGB estimation of trees in plantation forest is of great significance for evaluating its carbon sequestration capacity and ecological service functions.

As an active remote sensing technology, light detection and ranging (LiDAR) has stronger penetrability and can overcome the problem of signal saturation in synthetic aperture radar (SAR) and optical remote sensing (Lu et al., 2014; Hu et al., 2016; Nie et al., 2017; Jiang et al., 2020; Su et al., 2020). It can obtain detailed information on the three-dimensional (3D) spatial structure of a forest and the underlying terrain (Popescu et al., 2002; Hilker et al., 2010; Li et al., 2016). Hence, it is a more effective tool to study the extraction of structure parameters of individual trees and the indirect estimation of forest AGB in various forest environments (Hu et al., 2016; Nie et al., 2017; Jiang et al., 2020; Lu et al., 2020; Xu et al., 2021). According to the carrying platform, LiDAR deployments can be classified into four types: space-borne laser scanner (SLS), airborne laser scanner (ALS), vehicle-borne laser scanner (VLS), and terrestrial laser scanner (TLS) (Wu et al., 2013; Chen et al., 2021). Due to the reference beam divergence, the footprint of individual pulses from SLS is on a scale of several meters in diameter (Gong et al., 2011; Sun et al., 2011), making it nearly impossible to identify individual trees in a forest. The platform movement of VLS can be blocked by floor obstacles (Beland et al., 2019), resulting in limited spatial coverage for the data collection of a forest. The poor mobility and complex field operations of TLS restrict repeated surveys for a large forest (Wu et al., 2013; Jiang et al., 2022). In contrast, ALS can provide accurate and dense measurements of multiple forest types with a large spatial coverage (Wu et al., 2013; White et al., 2016). Particularly, unmanned aerial vehicle (UAV)-borne LiDAR has the advantages of higher precision data, lower cost, and stronger maneuverability, and is optimal for forest AGB estimation at the single tree scale (Liu et al., 2018; Wu et al., 2019; Wang et al., 2020; Chen et al., 2021).

The tree biomass equation is the most common and efficient method for non-destructively estimating forest AGB at the individual tree scale (Alvarez et al., 2012; Chave et al., 2014; Paul et al., 2016; Luo et al., 2020) and is generally realized by establishing the allometric relationship between the structure parameters of individual trees and the AGBs. Theoretically, both trunk height (H) and diameter at breast height (DBH) affect the tree AGB (Allouis et al., 2011; Paul et al., 2016; Shi and Liu, 2017). DBH is the most pivotal and commonly used predictor in the allometric equations for tree AGB estimation (Alvarez et al., 2012; Paul et al., 2016; Fu et al., 2018), but it cannot be directly obtained using UAV-borne LiDAR (Allouis et al., 2011; Wu et al., 2013; Lu et al., 2020; Xu et al., 2021). H can be directly and accurately extracted from the UAV LiDAR data (Wallace et al., 2014; Liu et al., 2018; Lu et al., 2020; Ma et al., 2022) and can be utilized as the only predictor to construct the allometric equation to estimate the tree AGB (Blujdea et al., 2012; Goodman et al., 2013; Lin et al., 2018). However, the single parameter H will unavoidably introduce uncertainties into the resulting AGB. The structure parameters reflecting the size and shape of the tree crown (e.g., crown height, crown width, crown diameter, crown projection area, crown surface area, and crown volume) have also exhibited certain allometric relationship with the H/DBH of a single tree (Li, 2019). Therefore, several researchers have tried incorporating crown parameters into the AGB estimation (Popescu, 2007; Wan-Mohd-Jaafar et al., 2017; Liu et al., 2021; Lin et al., 2022) and achieved improved accuracies. However, unlike the DBH, the crown parameters were seriously affected by neighboring trees, especially in a natural forest with multiple tree species and uneven ages. Hence, it will inevitably introduce uncertainties into the estimated AGB using crown parameters. This problem has been greatly weakened in plantation forests, which are intensively managed, comprise only one or two tree species, are even-aged, and are planted at regular spacing (FAO, 2020).

Nevertheless, not all crown parameters are suitable to be combined with trunk height to estimate the tree AGB of a plantation forest. As the point cloud is scanned by UAV-borne LiDAR from the air, it is difficult to obtain those structure parameters involving the crown base, including crown height, crown surface area, and crown volume (Wu et al., 2013; Beland et al., 2019; Xu et al., 2021). As for crown width and diameter, they are more suitable for trees with relatively symmetrical crowns. In contrast, the crown area (A_c) can not only be accurately extracted from the UAV LiDAR data through individual tree segmentation (Kuyah et al., 2012; White et al., 2016; Xu et al., 2021) but can also well reflect the size and shape of tree crowns. Although relatively uniformly distributed in the plantation forest, the individual trees at different positions (in the interior or at the edge) are shaded or squeezed to different extents by adjacent tree crowns. Hence, the A_cs of trees with similar trunk heights are not always approximate. Under undisturbed growth conditions, the A_c and H/DBH of an individual tree also have a certain allometric relationship (Allouis et al., 2011; Fu et al., 2018; Li, 2019). Therefore, it is expected to further enhance the precision of AGB estimation based on A_c and H by correcting the initial A_cs of trees in a plantation forest according to a unified rule.

In this article, we aim to apply the UAV LiDAR data to extract and correct A_c and construct a novel allometric model based on corrected A_c (A_{cc}) and H to precisely calculate the AGB of plantation trees. The specific objectives comprise (1) establishing the allometric model based on H to retrieve the potential maximum A_c of an individual tree under undisturbed growth conditions, and then combining the initial A_c extracted from the LiDAR point cloud to derive the A_{cc} with the correction equation; (2) constructing the allometric model with predictors of A_{cc} and H to more precisely estimate the AGB of plantation trees with UAV-borne LiDAR.

2. Test site and materials

2.1. Test site

Located in the Beibei District of Chongqing municipality in southwest China and close to Jinyun Mountain and Jialing River (Figure 1a), the test site has elevations varying from 164.52 m to 174.06 m (Figure 1b). This region has the characteristics of

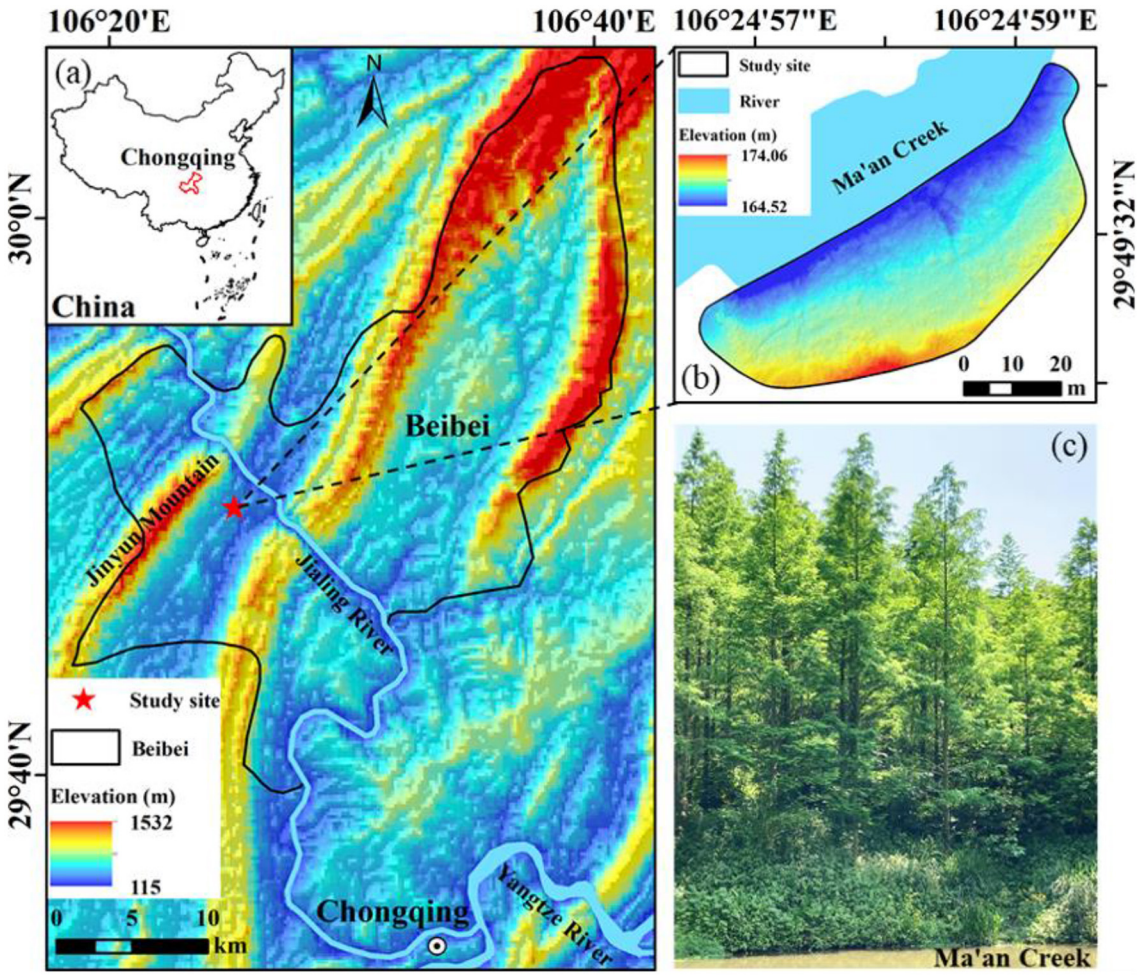

FIGURE 1
(a) Spatial location of the test site; **(b)** terrain of the test site rendered by elevation; **(c)** sample DR trees from the horizontal perspective.

a moist monsoon climate in the subtropics, with an average yearly temperature of 18°C and an average yearly precipitation of 1156 mm. The research target is one plot of plantation trees planted along Ma'anxi Creek, and the dawn redwood (DR for short, *Metasequoia glyptostroboides Hu and Cheng*) is the only tree species. Some shrubs and weeds were sporadically distributed underneath the trees (Figure 1c). Due to its characteristics of fast growth, high yield, forest formation, and strong adaptability, the DR tree has been widely cultivated around the world and categorized as one of the principal afforestation tree species in China (Ma, 2007). The DR trees in the test site grow in their natural state and are nearly planted with regular spacing. Their crowns have a steeple-like shape from the horizontal perspective and a nearly circular shape from the vertical perspective. Hence, it is an appropriate site to study the allometric model with A_{cc} and H as predictors for precisely estimating the AGBs of plantation trees.

2.2. UAV LiDAR data

In this study, the FEIMA D2000 equipped with D-LiDAR2000 (Figure 2A) was used to scan the test site. The quad-rotor drone has a maximum take-off weight of 3.35 kg and a maximum load of 750 g. The LiDAR system is a light-weight and high-precision airborne laser sensor with a weight of 680 g, a measurement accuracy of up to 3 cm (50 m flight height), three returns of each pulse, and a point frequency of 240 ktps/s. Prior to UAV flight, the technical parameters were preset as follows: the flight trajectory was a cross one (Figure 2B), the flight height was 80 m above the ground, both the longitudinal and lateral overlap were 80%, the flight speed was 5 m/s, and the scanning mode was area scanning. The raw data acquired by the laser scanner were processed using the included software to produce a LAS-formatted point cloud with the coordinate system of WGS84/UTM Zone 48N and a point density of about 2,800 points/m^2 (Figure 2C).

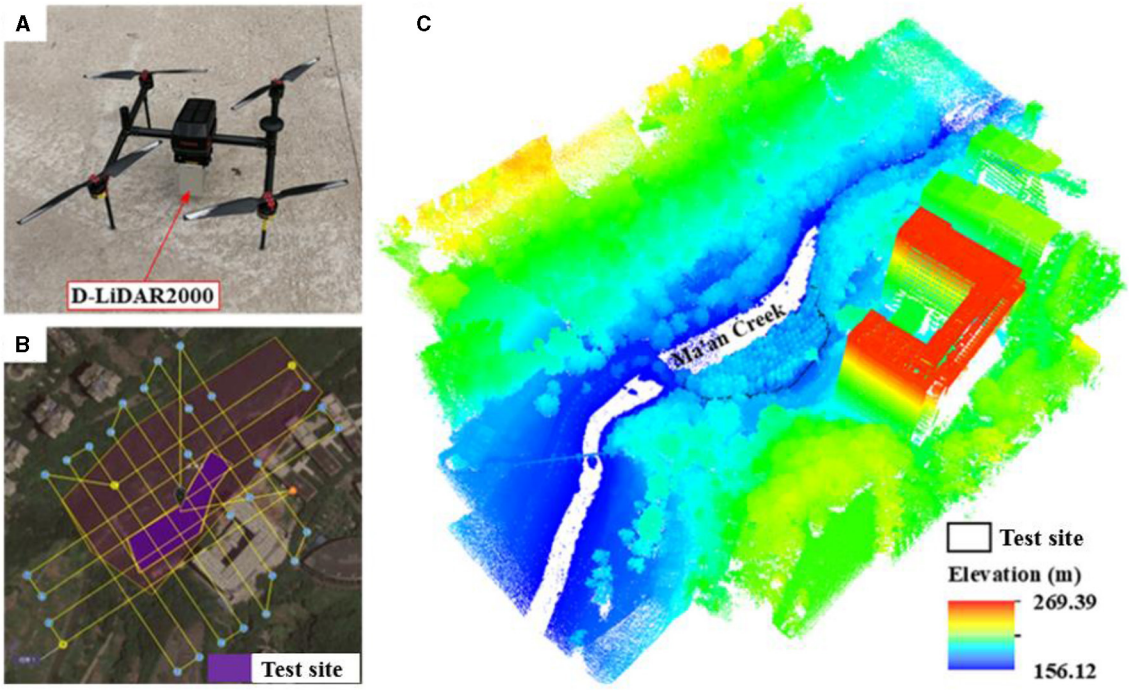

FIGURE 2
(A) UAV-borne LiDAR system; **(B)** cross-flight trajectory; **(C)** resulting 3D point cloud.

2.3. Field-measured data

The data measured in the field were crucial to establishing an allometric model and assessing the accuracy of the estimated AGBs. As shown in Figure 3C, 60 DR trees were selected as samples in this study. Among them, 15 trees marked with cyan points (ID: 1–15) were used for crown area correction, 30 with black points (ID: 16–45) were for fitting biomass models, and 15 trees with white points (ID: 46–60) were for accuracy evaluation. The DBHs and Hs of all sample trees were measured using a total station (Figure 3A) and a DBH tape (Figure 3B) separately and are shown in Table 1.

3. Methods

To combine A_c and H to accurately estimate AGBs of DR trees in the test site, the accurate A_c and an applicable allometric model with predictors of corrected A_c and H are required. The point cloud was first normalized using a digital elevation model (DEM), which was produced from the filtered ground points. Second, the seed points were generated from the canopy height model (CHM), which was obtained from classified vegetation points. Third, individual trees were segmented from the normalized point cloud using seed points, and their Hs and initial A_cs were extracted. Fourth, the equation for retrieving the potential maximum A_c of an individual tree under undisturbed growth conditions was established using the derived maximum A_c and measured H of those sample trees on the riverside. Fifth, the retrieved maximum A_cs and the initial A_cs of all other trees were combined to acquire the corrected A_cs using the correction equation. Finally, the AGBs of sample DR trees for model fitting were calculated using field-measured DBHs and Hs and integrated with the corresponding corrected A_cs and measured Hs to construct the novel allometric model. Thus, the AGBs of DR trees in the test site could be achieved by importing the corrected A_cs and obtained Hs into the newly constructed allometric model. The entire flow chart is illustrated in Figure 4.

3.1. Point cloud normalization

To eliminate the influence of topographic relief, the values in the *Z*-axis of non-ground points would be normalized from altitudes relative to sea level to heights relative to the ground. Before normalization, the LiDAR point cloud (Figure 2C) was tailored to the test site and removed noise points. The ground points were separated using the enhanced progressive TIN (triangulated irregular network) densification algorithm (Zhao et al., 2016). The point cloud was first gridded, and the lowest points in grid cells were used as seed points to establish the initial TIN. Then it was densified on a layer-wise basis via iterated processing until each ground point meeting the thresholds of iterative distance and angle (1.4 m and 20°) was found. Subsequently, the resulting ground points were utilized to produce a raster DEM with the IDW (inverse distance weighting) interpolation method. Finally, the normalization was accomplished by subtracting the elevations of the corresponding DEM pixels from those of non-ground points. Then, the normalized points were separated into low, medium, and high vegetation in accordance with the height separation points of 2 m and 5 m (ASPRS, 2005).

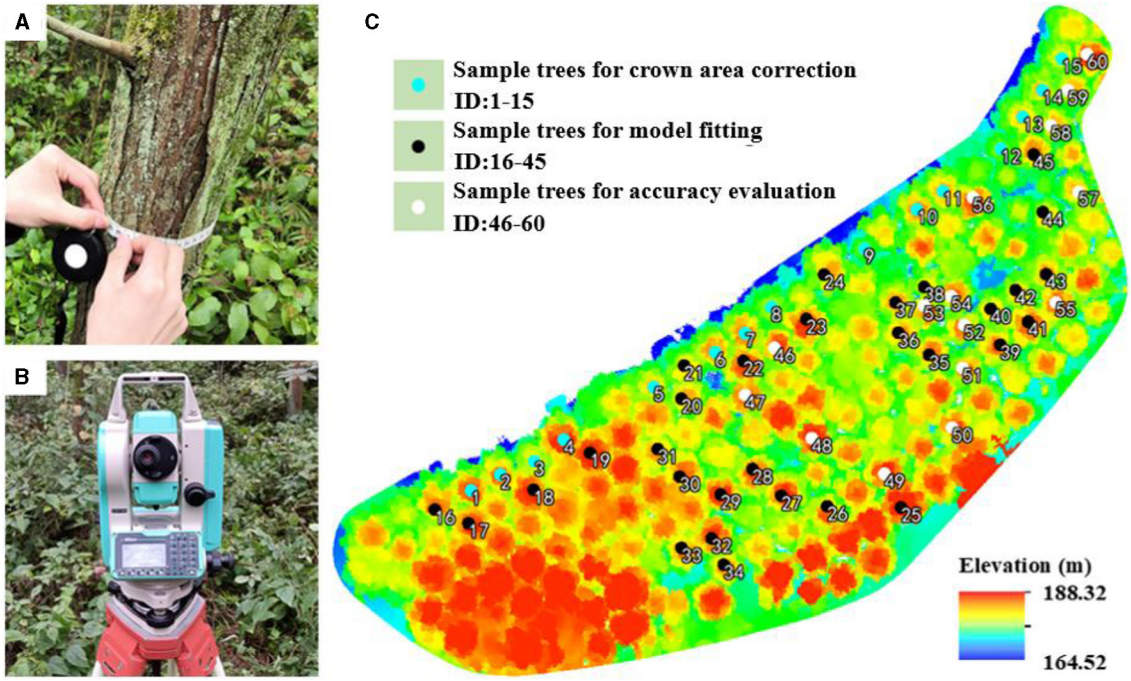

FIGURE 3
Field measurement: **(A)** DBH tape for measuring DBH; **(B)** total station for measuring H; **(C)** spatial distribution of sample DR trees in the test site.

TABLE 1 **Field-measured DBHs and Hs of sample DR trees in the test site.**

Tree ID	H (m)	DBH (cm)	Tree ID	H (m)	DBH (cm)	Tree ID	H (m)	DBH (cm)	Tree ID	H (m)	DBH (cm)
1	16.12	18.06	**16**	15.82	19.26	**31**	12.95	14.96	**46**	15.71	17.51
2	15.31	18.46	**17**	15.24	19.26	**32**	12.43	15.41	**47**	14.07	16.07
3	12.58	15.22	**18**	15.04	19.99	**33**	11.32	14.15	**48**	15.35	17.65
4	16.94	20.53	**19**	15.94	20.92	**34**	10.56	12.51	**49**	14.43	17.06
5	13.83	18.37	**20**	13.36	15.76	**35**	13.36	16.71	**50**	12.99	13.31
6	15.62	19.26	**21**	13.70	18.62	**36**	13.39	16.55	**51**	12.59	13.05
7	15.76	19.74	**22**	15.50	18.94	**37**	13.58	16.23	**52**	12.99	13.85
8	11.97	15.60	**23**	16.13	19.54	**38**	11.14	12.71	**53**	13.26	14.01
9	10.81	12.65	**24**	15.33	21.80	**39**	13.16	14.87	**54**	13.78	15.28
10	15.80	19.32	**25**	16.46	21.49	**40**	11.70	12.89	**55**	13.37	14.16
11	14.97	20.12	**26**	11.85	14.90	**41**	13.40	18.14	**56**	15.96	18.59
12	11.40	13.43	**27**	14.23	20.44	**42**	11.38	13.21	**57**	11.71	12.10
13	14.28	18.53	**28**	13.38	17.89	**43**	12.56	15.60	**58**	13.72	14.36
14	15.08	17.41	**29**	14.53	18.14	**44**	11.50	13.85	**59**	13.15	14.74
15	13.20	15.92	**30**	12.43	13.37	**45**	14.72	18.40	**60**	16.13	16.74

Tree ID 1–15 were for crown area correction, 16–45 for model fitting, and 46–60 for accuracy evaluation.

3.2. Seed point generation

It will improve the accuracy of segmenting individual trees from the point cloud by using tree tops as seed points. The local maxima filter (Wulder et al., 2000) is the most typical and widely applied method for tree top detection. The idea of this method is to utilize a moving window to search for the points with the local maximum heights as tree tops. In this study, a raster CHM was first produced from the classified vegetation points. In light of field survey and measurement, the heights to crown bases (HCB) of DR trees in the test site were no <2.5 m. Hence, the CHM pixels, which had

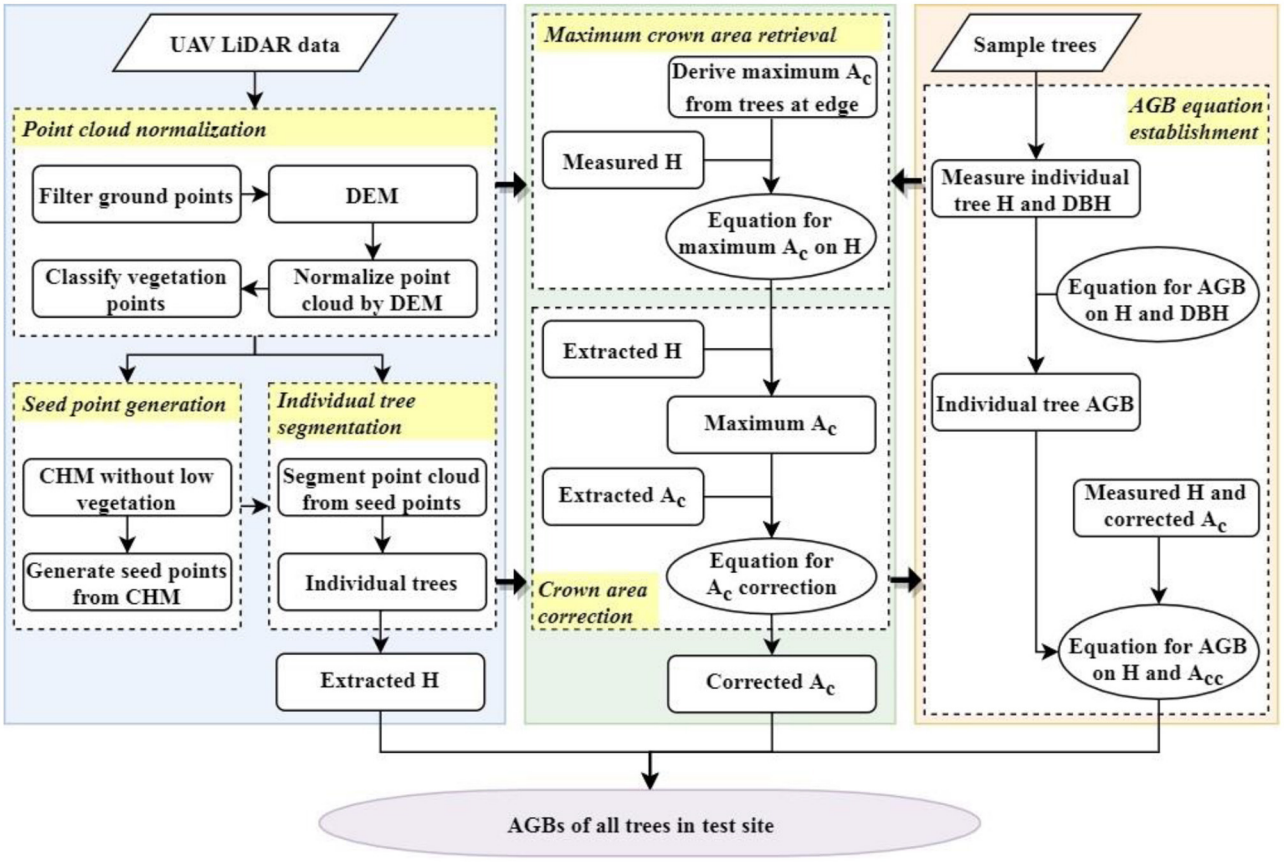

FIGURE 4
Flow chart of extracting and correcting crown area to precisely estimate AGBs of trees in plantation forest with UAV LiDAR data.

values lower than 2.5 m, would be deleted to eradicate the low vegetation (shrubs and weeds). Afterward, the seed points were generated by detecting the local maximum heights in the rest of the CHM pixels through a suitable moving window, whose size was determined by the crown size and stand structure characteristics.

3.3. Individual tree segmentation

Individual tree segmentation is the prerequisite for extracting tree-scale parameters, including trunk height and crown area. In this study, the segmentation algorithm developed by Li et al. (2012) was adopted to segment individual trees out of the point cloud acquired by the UAV-borne LiDAR. The points of two neighboring trees were sequentially separated and assigned from top to bottom according to the specified spacing threshold, minimal spacing rule, and planar outlines of tree crowns. It is very critical to appropriately set the spacing threshold. When it is too large or too small, the phenomenon of under-segmentation or over-segmentation will appear. The common practice is to set the maximum crown radius in the test site as the spacing threshold. The seed points generated in the previous subsection were used as individual tree tops. The normalized elevations of these tree tops were actually their Hs. The individual DR trees were eventually segmented, and the point cloud of each tree was separately projected onto a 2D plane to generate the minimum convex hull. The resulting polygon was considered the crown outline, and thus its area was the A_c of the tree.

3.4. Crown area correction

According to the field investigation, the branches of adjacent DR trees in the test site overlapped each other in various degrees at different positions (in the interior or at the edge). As a response, the sizes and shapes of crowns were usually reduced and changed on the parts shaded and squeezed by adjacent crowns. As indicated in Figure 5A, tree T1 was at the edge of the forest (on the riverside), and tree T2 was in the interior. The branches of T1 on the riverside grew unrestricted, but those on the other side seriously overlapped with T2. Although T2 was slightly taller than T1, the A_c of T2 was smaller than that of T1 (Figure 5B). Hence, it was a good practice to correct the initial A_cs of trees with reference to the maximum A_cs of trees growing under undisturbed conditions. The allometric relationship between the potential maximum A_c and the height of an individual tree needed to be constructed.

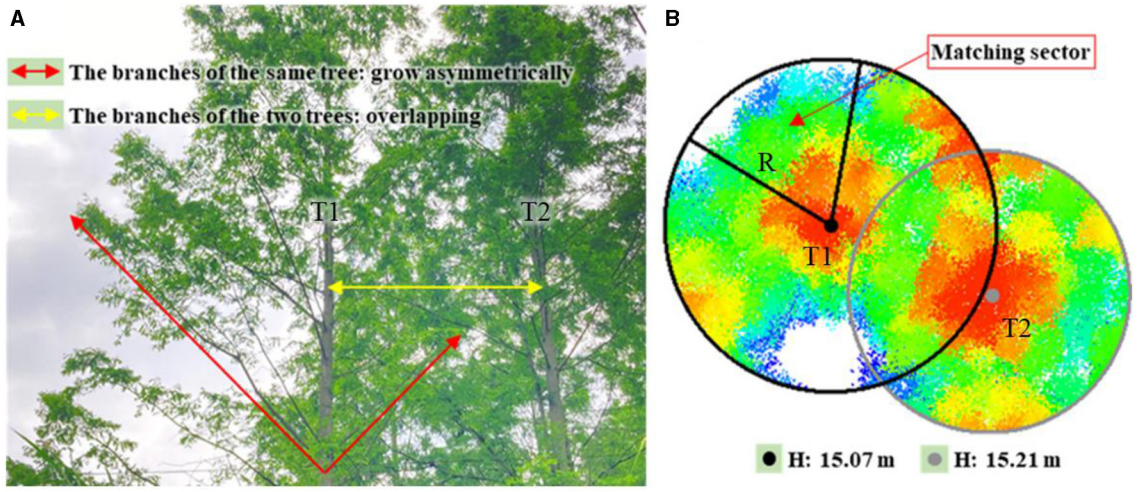

FIGURE 5
(A) Overlapping crowns of tree T1 at the edge and T2 in the interior of the plantation forest; **(B)** unrestricted growth part of T1 crown was extracted using a matching sector.

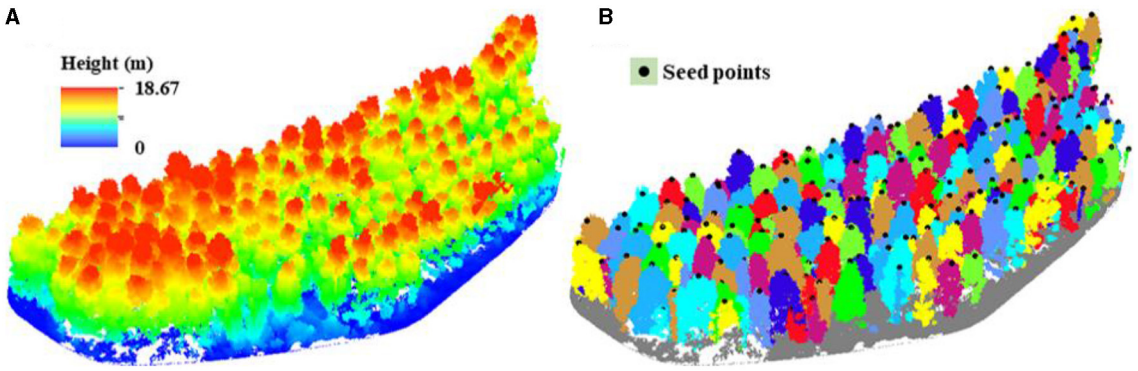

FIGURE 6
(A) Normalized UAV LiDAR point cloud of the test site; **(B)** identified individual DR trees with seed points.

Since there were no DR trees completely undisturbed by neighboring trees in the test site, the maximum A_cs could not be directly obtained. As the growth of a tree crown at the forest edge was frequently unrestricted in the outward direction, the outward part of the crown could proportionally derive an entire A_c that would be taken as the potential maximum A_c of the tree. As shown in Figure 5B, the tree top of T1 was used as the center to create a circumcircle covering the entire tree crown, and then the unrestricted growth part of the crown was extracted using a matching sector. Afterward, the potential maximum A_c of T1 could be calculated using Eq. (1).

$$\frac{A_{cmax}}{A_{cs}} = \frac{\pi R^2}{S} \quad (1)$$

where A_{cmax} is the potential maximum A_c of a tree (m^2), A_{cs} is the area of the unrestricted part of the crown extracted by the matching sector (m^2), R represents the radius of the circumcircle (m), and S represents the area of the matching sector (m^2).

In this study, the power function (Eq. 2) was determined as the allometric model for retrieving the maximum A_c under undisturbed growth conditions (see section 5.1 for comparisons with other allometric models). By fitting the Hs and calculating the maximum A_cs of sample trees (ID: 1–15) on the riverside with Eq. (2), the coefficient values would be determined. Thus, the maximum A_cs of all DR trees in the test site could be obtained by entering the extracted Hs into Eq. (2).

$$A_{cmax} = a \cdot H^b \quad (2)$$

where A_{cmax} is the maximum A_c of an individual tree (m^2), a and b are model coefficients, and H is the extracted trunk height from the point cloud (m).

Affected by adjacent crowns, the actual crown size of a DR tree would shrink to a certain degree, and the corresponding AGB would be slightly reduced. Therefore, the final A_c

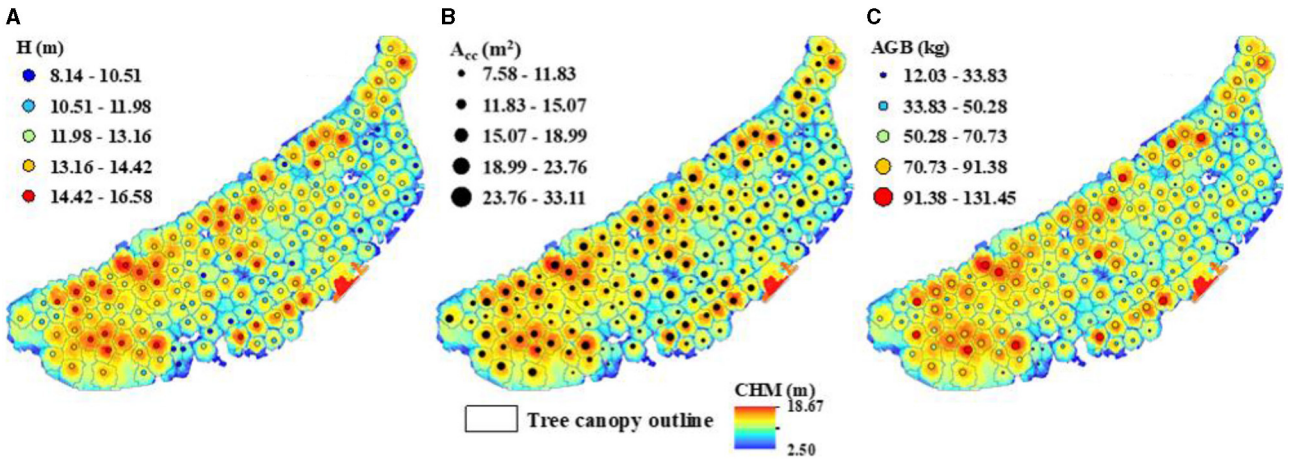

FIGURE 7
Segmented individual DR trees in the test site: **(A)** Hs extracted from UAV LiDAR data; **(B)** A_{cc}s calculated on maximum A_c and initial A_c; **(C)** the AGBs estimated on H and A_{cc}.

TABLE 2 Hs and initial A_cs of sample DR trees extracted from UAV LiDAR data.

Tree ID	H (m)	A_c (m²)	Tree ID	H (m)	A_c (m²)	Tree ID	H (m)	A_c (m²)	Tree ID	H (m)	A_c (m²)
1	15.56	17.22	**16**	14.65	24.42	**31**	12.38	9.73	**46**	15.18	13.53
2	15.05	18.67	**17**	14.68	18.63	**32**	12.89	17.81	**47**	13.65	15.01
3	12.96	11.56	**18**	14.79	19.19	**33**	11.48	12.50	**48**	14.87	20.92
4	16.58	27.07	**19**	15.38	19.55	**34**	10.39	14.57	**49**	14.39	19.73
5	13.51	17.28	**20**	13.03	14.57	**35**	13.09	16.51	**50**	12.58	13.36
6	15.07	19.68	**21**	13.14	17.28	**36**	12.89	16.08	**51**	11.98	16.74
7	15.20	17.07	**22**	15.21	18.35	**37**	13.09	18.50	**52**	12.79	14.59
8	11.57	15.62	**23**	15.66	21.43	**38**	10.85	9.33	**53**	12.53	12.03
9	10.32	9.13	**24**	14.66	26.85	**39**	12.86	17.08	**54**	13.16	15.87
10	15.26	21.46	**25**	15.75	21.83	**40**	11.31	11.80	**55**	12.51	17.12
11	14.42	20.47	**26**	11.98	15.37	**41**	12.94	24.41	**56**	15.70	19.96
12	10.66	11.99	**27**	13.70	23.94	**42**	11.18	11.21	**57**	11.23	12.37
13	13.83	24.03	**28**	13.09	20.56	**43**	12.11	17.36	**58**	13.29	15.19
14	14.42	16.33	**29**	14.04	19.83	**44**	10.88	16.06	**59**	12.54	12.29
15	12.49	14.82	**30**	12.87	15.37	**45**	13.89	17.58	**60**	15.52	13.81

Tree ID 1–15 were sample trees for crown area correction, 16–45 for model fitting, and 46–60 for accuracy evaluation.

that was used to estimate the tree AGB should be a value between the maximum A_c and the initial A_c. Through repeated experiments, Eq. (3) was proposed as the empirical equation for crown area correction and demonstrated sound performance in estimating the AGBs of single DR trees in the test site.

$$A_{cc} = A_{cmax} \cdot \exp^{\left(\frac{A_c}{A_{cmax}}\right)-1} \quad (3)$$

where A_c is the crown area of an individual tree initially extracted from a point cloud (m²), A_{cc} is the corrected A_c of the tree (m²), and A_{cmax} is the potential maximum A_c of the tree (m²).

3.5. Allometric model for tree AGB estimation

According to the biomass models for China's tree species (Luo et al., 2020), the allometric model on DBH and H suitable for calculating the AGB of individual DR trees in the test site is as follows:

$$W = 0.05488 \cdot (D^2 H)^{0.8583} \quad (4)$$

where W is single tree AGB (kg), D is trunk DBH (cm), and H is trunk height (m).

TABLE 3 R, S, A_{cs}, A_{cmax}, and A_c of sample DR trees (ID: 1–15) on the riverside for crown area correction.

Tree ID	R (m)	S (m^2)	A_{cs} (m^2)	A_{cmax} (m^2)	A_c (m^2)	Tree ID	R (m)	S (m^2)	A_{cs} (m^2)	A_{cmax} (m^2)	A_c (m^2)
1	3.5	2.99	2.39	30.74	19.80	**9**	2.50	2.18	1.71	15.36	10.24
2	3.5	4.81	3.47	27.78	20.02	**10**	3.50	7.38	6.18	32.21	23.07
3	3.0	3.69	2.84	21.73	13.61	**11**	3.50	7.17	5.03	27.00	21.20
4	4.0	12.29	8.80	35.98	28.09	**12**	2.50	2.62	2.31	17.35	12.74
5	3.0	3.77	3.46	25.95	18.58	**13**	3.50	4.92	3.62	28.29	24.33
6	3.5	6.30	5.01	30.63	21.42	**14**	3.50	2.99	2.20	28.31	18.54
7	3.5	5.24	4.01	29.48	19.35	**15**	3.50	4.17	2.69	24.81	16.59
8	3.0	4.79	3.41	20.13	16.09						

R was the radius of the circumcircle, S was the area of the matching sector, A_{cs} was the A_c contained in the matching sector, A_{cmax} was the potential maximum A_c, and A_{cc} was the corrected A_c.

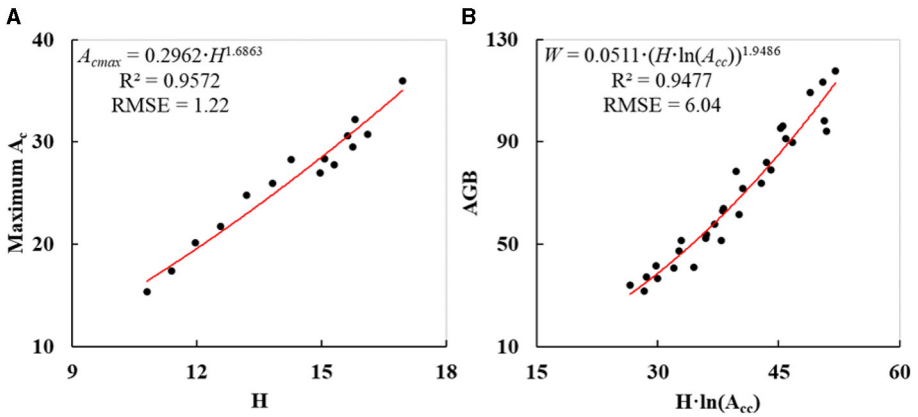

FIGURE 8
Fitted curves of individual DR trees: **(A)** potential maximum A_c derived on H; **(B)** AGB estimated on A_{cc} and H.

Accordingly, the AGB of DR trees (ID: 16–45) for model fitting could be obtained by putting their measured Hs and DBHs into Eq. (4).

As the H could be conveniently obtained from UAV LiDAR data and the A_{cc} could be calculated using Eqs. (2, 3) the quantitative relation between A_{cc}, H, and AGB was required to be established. The power function (Eq. 5) was determined to be the novel allometric model for AGB estimation in the study (see section 5.2 for comparison with other allometric models).

$$W = \alpha \cdot (H \cdot \ln(A_{cc}))^{\beta} \quad (5)$$

where W is the individual tree AGB (kg), α and β are model coefficients, H is trunk height (m), and A_{cc} is the corrected A_c of the tree (m^2).

By fitting the extracted Hs, corrected A_cs, and estimated AGBs of sample trees (ID: 16–45) with Eq. (5), model coefficients α and β could be ascertained, and the allometric model with predictors of A_{cc} and H for AGB estimation would be constructed. Hence, the AGB of each DR tree in the test site could be achieved by putting the corrected A_c and extracted H into the new allometric model.

4. Results

4.1. Generated seed points

The noise points were first cleaned from the point cloud of the test site using the software LiDAR360 (https://www.lidar360.com/). Then, the cleaned point cloud was normalized as Figure 6A, which represented the surface characteristics of tree crowns. The two key factors affecting seed point generation were the resolution of CHM and the size of the moving window for filtering the local maxima. Through repeated experiments, the CHM with a resolution of 0.3 m was appropriate for this purpose. With consideration of approximately round crown outlines and the maximum radius of DR tree crowns in the test site, a circle with a radius of 3 m was utilized to detect the local maxima of the CHM and generate seed points. According to the field survey, there were 154 DR trees in the test site. However, in order to avoid over-segmentation (e.g., crown overlap) and under-segmentation (e.g., no gap between trees due to lower vegetation occlusion), 192 local maximum pixels were finally marked as seed points (Figure 6B) to improve the segmentation accuracy.

TABLE 4 A_{cmax} and A_{cc} of sample DR trees for model fitting (ID: 16–45) and accuracy evaluation (ID: 46–60).

Tree ID	A_{cmax} (m^2)	A_{cc} (m^2)	Tree ID	A_{cmax} (m^2)	A_{cc}(m^2)	Tree ID	A_{cmax} (m^2)	A_{cc} (m^2)	Tree ID	A_{cmax} (m^2)	A_{cc} (m^2)
16	31.18	25.10	**28**	23.52	20.74	**40**	18.74	12.94	**52**	22.35	15.79
17	29.27	20.35	**29**	27.01	20.70	**41**	23.56	24.42	**53**	23.14	14.32
18	28.63	20.59	**30**	20.76	16.01	**42**	17.88	12.31	**54**	24.70	17.28
19	31.56	21.57	**31**	22.26	12.68	**43**	21.13	17.67	**55**	23.49	17.91
20	23.45	16.06	**32**	20.76	18.01	**44**	18.20	16.18	**56**	31.66	21.88
21	24.46	18.24	**33**	17.72	13.20	**45**	27.59	19.20	**57**	18.77	13.35
22	30.12	20.38	**34**	15.76	14.62	**46**	30.81	17.59	**58**	24.53	16.76
23	32.23	23.05	**35**	23.44	17.44	**47**	25.57	16.92	**59**	22.83	14.38
24	29.56	26.97	**36**	23.55	17.15	**48**	29.63	22.08	**60**	32.22	18.20
25	33.32	23.60	**37**	24.10	19.10	**49**	26.70	20.57			
26	19.14	15.72	**38**	17.25	10.90	**50**	22.37	14.95			
27	26.08	24.03	**39**	22.87	17.75	**51**	21.20	17.18			

A_{cmax} was the potential maximum A_c, and A_{cc} was the corrected A_c.

4.2. Segmented individual trees

According to field observation and measurement, the Hs, HCBs, and crown radiuses of DR trees in the test site were no <5 m, no <2.5 m, and no more than 3 m, respectively. Therefore, the normalized point cloud was used to segment individual trees based on seed points, with a minimum trunk height of 5 m, an aboveground height of 2.5 m, and a spacing threshold of 3 m. As a result, 154 DR trees in the test site were correctly identified (Figure 6B), and their Hs and initial A_cs were also obtained. The extracted Hs ranged from 8.14 m to 16.58 m (Figure 7A), with an average value of 12.74 m. The extracted initial A_cs and Hs of DR trees in the test site are listed in Table 2.

4.3. Corrected crown areas

To obtain the potential maximum A_cs of sample DR trees (ID: 1–15) on the riverside for crown area correction, the radiuses of their crown circumcircles, the areas of the matching sectors, and the parts of crown areas contained in the matching sectors were input into Eq. (1). The three parameters and the resulting maximum A_cs were listed in columns R, S, A_{cs}, and A_{cmax} of Table 3. Then, the calculated maximum A_cs and the measured Hs in Table 1 were utilized to fit Eq. (2). The model coefficients a and b were ascertained as 0.2962 and 1.6863, respectively. Thus, the allometric model for retrieving the potential maximum A_c of a DR tree under undisturbed growth conditions based on H was as follows:

$$A_{cmax} = 0.2962 \cdot H^{1.6863} \tag{6}$$

where A_{cmax} is the potential maximum A_c of a single tree (m^2), and H is the trunk height (m).

As indicated in Figure 8A, the coefficient of determination (R^2) of individual tree A_{cmax}s derived by Eq. (6) was 0.9572, and root mean square error (RMSE) was 1.22 m^2. Since R^2 was so close to 1.0 and RMSE was far below the mean A_c of 26.37 m^2, the potential maximum A_c and the measured H were soundly fitted.

The extracted Hs of other DR trees in the test site were input into Eq. (6) to obtain the corresponding maximum A_cs. Then the calculated maximum A_cs and the initial A_cs extracted by individual tree segmentation were input into Eq. (3) to obtain the finally corrected A_cs of all DR trees in the test site (Figure 7B). The corrected A_cs varied from 7.58 m^2 to 33.11 m^2, with a mean value of about 17.32 m^2. The maximum A_cs and corrected A_cs of sample trees (ID: 16–60) were listed in columns A_{cmax} and A_{cc} of Table 4, respectively. Compared with the initially extracted A_c, the corrected A_c increased by 1.29 m^2 on average.

4.4. Estimated AGBs

The AGBs of DR trees in Table 5 for model fitting were first calculated with Eq. (4) based on the measured DBHs and Hs in Table 1. Then, the estimated AGBs and their corresponding measured Hs in Table 1 and the corrected A_c in Table 4 were utilized to fit Eq. (5). The model coefficients α and β were ascertained as 0.0511 and 1.9486, respectively. Thus, the allometric model for estimating the DR tree AGB according to corrected A_c and H was as follows:

$$W = 0.0511 \cdot (H \cdot \ln(A_{cc}))^{1.9486} \tag{7}$$

where W is the tree AGB (kg), H is the trunk height (m), and A_{cc} is the corrected A_c of the tree (m^2).

As indicated in Figure 8B, R^2 and RMSE of individual tree AGBs calculated by Eq. (7) were 0.9477 and 6.04 kg, respectively. Since R^2 was so close to 1.0 and RMSE was far below the mean AGB of 68.36 kg, the calculated AGB and the product of H and logarithmic A_{cc} were soundly fitted. Then, the extracted Hs and corrected A_cs of other DR trees were input into Eq. (7) to obtain their AGBs. The resulting AGBs varied from

12.03 kg to 131.45 kg (Figure 7C) with a mean value of 58.06 kg, and the AGB of DR trees in the test site was nearly 8.9 t in total.

4.5. Accuracy evaluation

In this study, the accuracy of trunk Hs extracted from the point cloud scanned by UAV-borne LiDAR was first evaluated. The Hs of sample DR trees (Figure 3C) are shown in Table 2, and the corresponding measured Hs are shown in Table 1. As indicated in Figure 9A, R^2 and RMSE of the resulting Hs were 0.9688 and 0.51 m, implying that the Hs extracted from UAV LiDAR data had sound accuracy. The A_cs of sample DR trees that were initially extracted and subsequently corrected are listed in Tables 2, 4, respectively.

For the purpose of evaluating the accuracy of calculated AGBs by the newly constructed allometric model on corrected A_c and H, the AGBs of sample DR trees (ID: 46–60) were calculated using Eqs. (4) and (7), respectively (Table 6). As indicated in Figure 9B, R^2 and RMSE were 0.9432 and 10.91 kg, implying a high correlation between the AGB calculated on A_{cc} and H and that on DBH and H.

TABLE 5 Calculated AGBs of sample DR trees using Eq. (4) for model fitting.

Tree ID	AGB (kg)	Tree ID	AGB (kg)	Tree ID	AGB (kg)
16	94.16	**26**	47.27	**36**	62.94
17	91.19	**27**	95.20	**37**	61.61
18	96.13	**28**	71.88	**38**	34.14
19	109.21	**29**	79.02	**39**	51.56
20	57.71	**30**	40.91	**40**	36.49
21	78.55	**31**	51.42	**41**	73.70
22	89.91	**32**	52.19	**42**	37.15
23	98.22	**33**	41.62	**43**	53.79
24	113.41	**34**	31.73	**44**	40.64
25	117.55	**35**	63.84	**45**	81.81

5. Discussion

5.1. Relationship between trunk height and crown area

In the study, the maximum A_c of a tree referred to the crown area of the tree that grew under undisturbed conditions and was used to correct the initial A_c to mitigate the impacts from adjacent trees. As the potential maximum A_cs of most trees could not be directly obtained, the power function with trunk height (H) as the base (Eq. 6) was suggested to retrieve them in section 3.4. It was based on the fact that the crown area of a tree exhibited a certain allometric relationship with H under undisturbed growth conditions (Enquist and Niklas, 2001; Hulshof et al., 2015; Shi and Liu, 2017). The fitting data for the maximum A_c retrieval model were frequently collected from the trees at the edge or in sparsely distributed parts of the plantation forest. Actually, the other three possible retrieval models for the maximum A_c with the variable of "H" had also been tested, comprising exponential function, linear function, and logarithmic function. The measured Hs in Table 1 and the derived maximum A_cs in Table 3 of sample trees (ID: 1–15) were utilized to fit them separately. The fitting degree has a positive correlation with the value of R^2. The fitted curves are indicated in Figures 10A–C, and the resulting R^2 were 0.9433, 0.954, and 0.9545. R^2 of all models demonstrated a good positive relationship between potential maximum A_c and H, which was in accordance with other studies (Liu et al., 2019; Zhao et al., 2021). With the highest R^2, the power function model adopted in this study (Eq. 6) was optimal for expressing the allometric growth relationship between the potential maximum A_c and H.

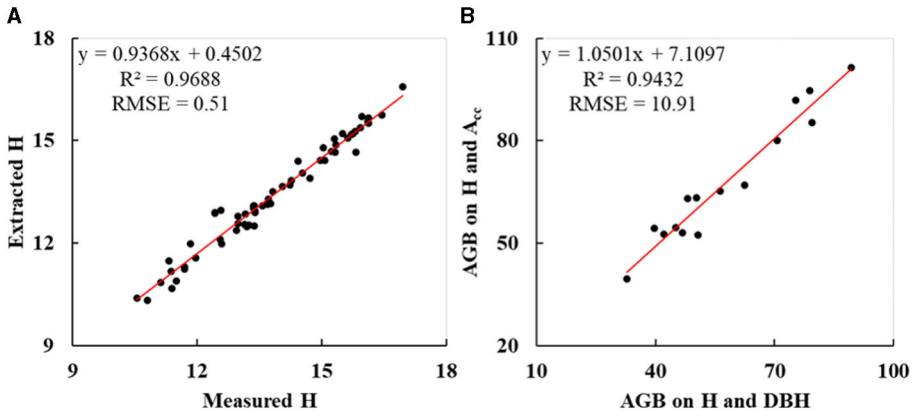

FIGURE 9
Accuracy evaluation of sample DR trees: **(A)** Hs extracted from UAV LiDAR data; **(B)** AGBs estimated on H and A_{cc}.

5.2. Comparison of various allometric models for tree AGB estimation

To achieve a precise AGB calculation of plantation trees, it is significant to construct a suitable allometric model with predictors that could be obtained by UAV-borne LiDAR. According to section 3.5, the power function with "H · ln(A_{cc})" as the base was suggested as the allometric model. In fact, nine other potential allometric models were also experimented. The field-measured Hs in Table 1, initial A_cs in Table 2 or corrected A_cs in Table 4, and calculated AGBs in Table 5 of sample DR trees (ID: 16–45) (Figure 3C) were utilized to fit them separately. The allometric equation with the single predictor of H was suggested by Lin et al. (2018). The fitted curve is illustrated in Figure 11A with the R^2 of 0.928. As shown in Figure 11B, the initial A_c was replaced by the corrected A_c to fit Eq. (5), and the R^2 of the fitted curve was 0.9184. With regard to the power functions that depended on A_{cc} and H, a few more compositions were tried as the bases comprising "H·A_{cc}", "H+A_{cc}", "H+ln(A_{cc})", and "H·(ln(A_{cc}))^2". The fitted curves are indicated in Figures 11C–F, and the resulting R^2 were 0.9063, 0.8903, 0.9451, and 0.922. In addition, we fitted several other classical function models with the same base of "H·ln(A_{cc})" comprising exponential function, linear function, and logarithmic function. The fitted curves are indicated in Figures 11G–I, and the resulting R^2 were 0.9449, 0.9364, and 0.9133. Since the R^2 of the fitted curve in Figure 8B was 0.9477, the applied allometric model (Eq. 7) had the highest degree of model fitting. Compared with Figure 11B, the corrected A_c exhibited better performance in estimating AGBs of plantation forest trees than the uncorrected A_c. Additionally, three other allometric models in Figures 11E, G, H had a larger R^2 than the allometric model in Figure 11A. They demonstrated again that the AGB calculation of plantation trees on A_{cc} and H outperformed that depending solely on H.

TABLE 6 Resulting AGBs of sample DR trees for accuracy evaluation.

Tree ID	AGB_1 (kg)	AGB_2 (kg)	Tree ID	AGB_1 (kg)	AGB_2 (kg)
46	79.47	85.25	**54**	56.21	65.23
47	62.42	66.94	**55**	48.11	63.07
48	78.97	94.55	**56**	89.31	101.48
49	70.68	80.13	**57**	32.73	39.47
50	42.15	52.57	**58**	50.33	63.38
51	39.68	54.45	**59**	50.76	52.32
52	45.12	54.61	**60**	75.30	91.85
53	46.83	52.95			

AGB_1 was calculated using Eq. (4), and AGB_2 using Eq. (7).

5.3. Error analysis and possible enhancements

Though UAV-borne LiDAR was employed to obtain precise AGB estimation of DR trees in a plantation forest, certain factors may have affected the accuracy. For example, due to the fear of hitting high buildings near the test site (see Figure 2C), the aboveground flight altitude of the UAV was preset to 80 m. It would inevitably reduce the elevation accuracy of the point cloud scanned by LiDAR, ultimately affecting the accuracy of tree segmentation and height extraction. The measured DBHs and Hs of sample DR trees, which were taken as the truths for model fitting and verification, possibly had some systematic errors owing to the instrument quality and usage procedure. According to section 3.4, the crowns of those trees on the riverside were used to derive the potential maximum A_cs under undisturbed growth conditions. However, the unrestricted part of the crowns accounted for only a small part of the entire crowns, inevitably bringing certain errors to the resulting data. The AGBs of the sample DR trees were possibly not precisely achieved since we directly applied the allometric model and the corresponding coefficient values from the reference.

Despite all this, certain steps can be adopted to enhance the AGB estimation precision of plantation trees in specific application scenarios. For instance, the UAV flight altitude can be lowered to 40 m through fine operations on the premise of safety, thus improving the elevation precision

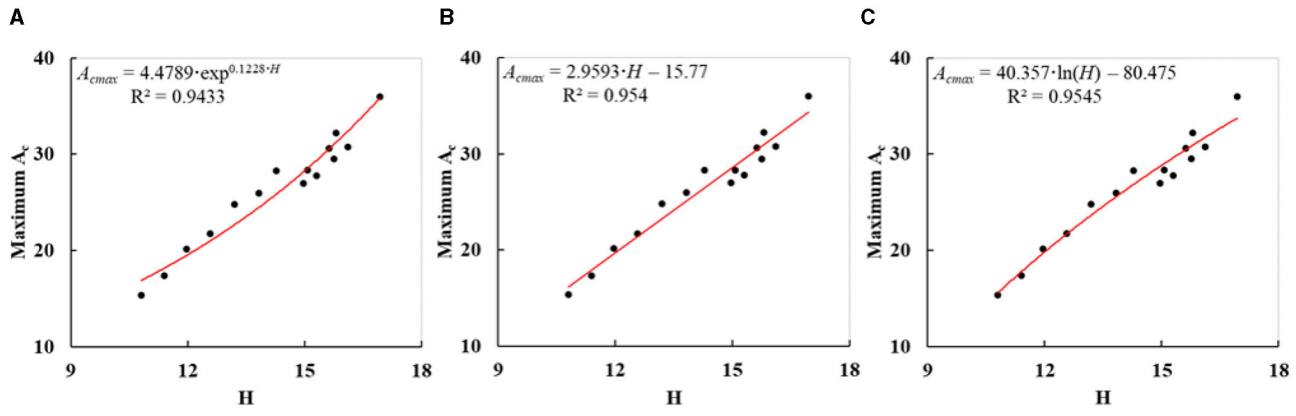

FIGURE 10
Fitted curves **(A–C)** of three other allometric models for retrieving the potential maximum A_c (A_{cmax}) based on H.

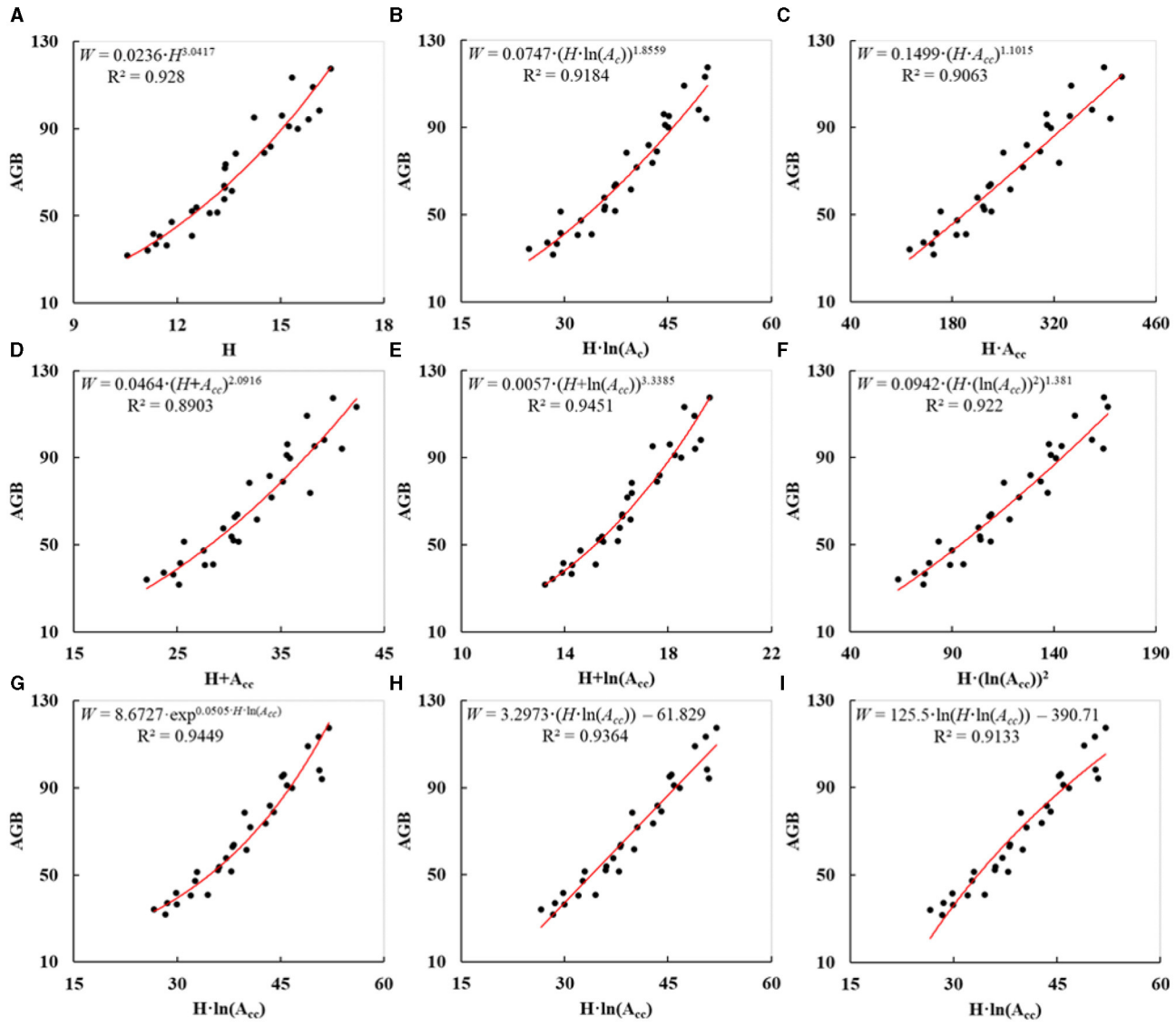

FIGURE 11
Fitted curves **(A–I)** of nine other allometric models for estimating AGBs of plantation trees.

of the resulting point cloud. The errors of field-measured data can be minimized by using standardized procedures and using the average value of multiple measurements. If possible, the sample trees whose entire crowns or the majority of crowns grew unrestricted should be selected to calculate the potential maximum A_cs. The coefficient values of the adopted allometric model on DBH and H can be ascertained via practical tests, rather than straightforward empirical ones for the DR species.

6. Conclusion

In this article, the UAV LiDAR data were utilized to extract and correct crown area for the precise AGB estimation of trees in a plantation forest. The following were the principal conclusions we drew:

- The approach of extracting and correcting A_c extracted from the UAV LiDAR data to precisely estimate the AGBs of plantation forest trees proved effective. The R^2 and RMSE of resulting AGBs of DR trees in the test site were 0.9432 and 10.91 kg.
- The unrestricted growth parts of the tree crowns at the edge of a plantation forest could be used to derive the potential maximum A_c. The power function model demonstrated the highest fitting degree between the potential maximum A_c and H, and the R^2 and RMSE were 0.9572 and 1.22 m^2, respectively.
- Compared with the allometric models for AGB estimation depending only on trunk H or on initial A_c and H, the novel allometric model proposed in this study was based on the predictor variables of corrected A_c and H and demonstrated superior performance in estimating the AGBs of trees in a plantation forest.

Though this study offers the applicable methodology to calculate the AGBs of individual DR trees in a plantation forest using UAV-borne LiDAR, certain reasons still impacted the precision, including excessive UAV flight altitude, systematic measurement errors, a lack of undisturbed crowns, and non-localized coefficients of the allometric model. Hence, it is always a real challenge to precisely achieve the AGBs of plantation trees with UAV LiDAR data.

Additionally, the crown area of a single tree in a plantation forest is mainly determined by tree spacing, species, and age. Therefore, the suitable spacing between trees should be kept while planting trees, and the crown overlap will be reduced and the trees will grow lusher. It also prevents the underneath branches and leaves from withering due to the lack of sunlight. Thus, the total AGBs of plantation forest trees will increase, and more carbon will be stored. Hence, it is very meaningful to study how to plan suitable spacing for the plantation forest trees to maximize the AGB and carbon sequestration. Meanwhile, the allometric relationship between DBH and the potential maximum A_c and the allometric models for AGB calculation of different tree species at various ages also need to be studied in future.

Data availability statement

The original contributions presented in the study are included in the article/supplementary material, further inquiries can be directed to the corresponding author.

Author contributions

JL: conceptualization, formal analysis, funding acquisition, investigation, methodology, writing—original draft, and writing—review and editing. DC: data curation, investigation, methodology, and writing—original draft. SY and XL: data curation and investigation. All authors read and approved the final version of the manuscript.

Funding

This study was partially sponsored by the National Natural Science Foundation of China (nos. 32071678 and 41830648) and the Key Research and Development Program of the Sichuan Province (no. 2022YFQ0035).

Conflict of interest

The authors declare that the research was conducted in the absence of any commercial or financial relationships that could be construed as a potential conflict of interest.

Publisher's note

All claims expressed in this article are solely those of the authors and do not necessarily represent those of their affiliated organizations, or those of the publisher, the editors and the reviewers. Any product that may be evaluated in this article, or claim that may be made by its manufacturer, is not guaranteed or endorsed by the publisher.

References

Allouis, T., Durrieu, S., Vega, C., and Couteron, P. (2011). "Exploiting fullwavefrom lidar signals to estimate timber volume and above-ground biomass of individual trees," in *2011 IEEE International Geoscience and Remote Sensing Symposium*. Vancouver, BC: IEEE, 1251–1254.

Alvarez, E., Duque, A., Saldarriaga, J., Cabrera, K., and Salas, G. D. (2012). Tree above-ground biomass allometries for carbon stocks estimation in the natural forests of Colombia. *For. Ecol. Manage.* 267, 297–308. doi: 10.1016/j.foreco.2011.12.013

ASPRS (2005). *LAS 1, 4. Specification Approved by ASPRS Board*. Available online at: https://www.asprs.org/divisions-committees/lidar-division/laser-las-file-format-exchange-activities (accessed June 26, 2022).

Beland, M., Parker, G., Sparrow, B., Harding, D., Chasmer, L., Phinn, S., et al. (2019). On promoting the use of lidar systems in forest ecosystem research. *For. Ecol. Manage.* 450, 117484. doi: 10.1016/j.foreco.2019.117484

Blujdea, V. N. B., Pilli, R., Dutca, I., Ciuvat, L., and Abrudan, I. V. (2012). Allometric biomass equations for young broadleaved trees in plantations in Romania. *For. Ecol. Manage.* 264, 172–184. doi: 10.1016/j.foreco.2011.09.042

Chave, J., Réjou-Méchain, M., Búrquez, A., Chidumayo, E., Colgan, M. S., Delitti, W. B. C., et al. (2014). Improved allometric models to estimate the aboveground biomass of tropical trees. *Glob. Change Biol.* 20, 3177–3190. doi: 10.1111/gcb.12629

Chen, D. M., Zhang, C. L., Wu, J. P., Zhou, L. X., Lin, Y. B., Fu, S. L., et al. (2011). Subtropical plantations are large carbon sinks: evidence from two monoculture plantations in South China. *Agric. For. Meteorol.* 151, 1214–1225. doi: 10.1016/j.agrformet.2011.04.011

Chen, Q., Laurin, G. V., and Valentini, R. (2015). Uncertainty of remotely sensed aboveground biomass over an African tropical forest: propagating errors from trees to plots to pixels. *Remote Sens. Environ.* 160, 134–143. doi: 10.1016/j.rse.2015.01.009

Chen, X. X., Jiang, K., Zhu, Y. S., Wang, X. J., and Yun, T. (2021). Individual tree crown segmentation directly from UAV-borne LiDAR data using the PointNet of deep learning. *Forests* 12, 131. doi: 10.3390/f12020131

Chen, Z., Dayananda, B., Fu, B., Li, Z. W., Jia, Z. Y., Hu, Y., et al. (2022). Research on the potential of forestry's carbon-neutral contribution in China from 2021 to 2060. *Sustainability* 14, 5444. doi: 10.3390/su14095444

Diao, J. J., Liu, J. X., Zhu, Z. L., Wei, X. Y., and Li, M. S. (2022). Active forest management accelerates carbon storage in plantation forests in Lishui, southern China. *For. Ecosyst.* 9, 100004. doi: 10.1016/j.fecs.2022.100004

Dubayah, R. O., Sheldon, S. L., Clark, D. B., Hofton, M. A., Blair, J. B., Hurtt, G. C., et al. (2010). Estimation of tropical forest height and biomass dynamics using lidar remote sensing at La Selva, Costa Rica. *J. Geophys. Res.-Biogeosci.* 115, G00E09. doi: 10.1029/2009JG000933

Dube, T., and Mutanga, O. (2016). The impact of integrating WorldView-2 sensor and environmental variables in estimating plantation forest species aboveground biomass and carbon stocks in uMgeni Catchment, South Africa. ISPRS-J. Photogramm. *Remote Sens.* 119, 415–425. doi: 10.1016/j.isprsjprs.2016.06.017

Enquist, B. J., and Niklas, K. J. (2001). Invariant scaling relations across tree-dominated communities. *Nature* 410, 655–660. doi: 10.1038/35070500

Fang, J. Y., Chen, A. P., Peng, C. H., Zhao, S. Q., and Ci, L. (2001). Changes in forest biomass carbon storage in China between 1949 and 1998. *Science* 292, 2320–2322. doi: 10.1126/science.1058629

FAO (2020). *Global Forest Resources Assessment 2020*. Available online at: https://www.fao.org/forest-resources-assessment/2020/en/ (accessed June 26, 2022).

Fu, L. Y., Liu, Q. W., Sun, H., Wang, Q. Y., Li, Z. Y., Chen, E. X., et al. (2018). Development of a system of compatible individual tree diameter and aboveground

biomass prediction models using error-in-variable regression and airborne LiDAR data. *Remote Sens*. 10, 325. doi: 10.3390/rs10020325

Gong, P., Li, Z., Huang, H. B., Sun, G. Q., and Wang, L. (2011). ICESat GLAS data for urban environment monitoring. IEEE Trans. Geosci. *Remote Sensing* 49, 1158–1172. doi: 10.1109/TGRS.2010.2070514

Goodman, R. C., Phillips, O. L., Torres, D. D., Freitas, L., Cortese, S. T., Monteagudo, A., et al. (2013). Amazon palm biomass and allometry. *For. Ecol. Manage*. 310, 994–1004. doi: 10.1016/j.foreco.2013.09.045

Guo, S., Zhao, H. B., Zhou, G. Y., Long, W. G., Gan, G. L., Wu, S. Y., et al. (2022). Biomass allocation of different species plantations in subtropical area of China. *For. Res*. 35, 182–189.

Hilker, T., van Leeuwen, M., Coops, N. C., Wulder, M. A., Newnham, G. J., Juup, D. L. B., et al. (2010). Comparing crown metrics derived from terrestrial and airborne laser scanning in a Douglas-fir dominated forest stand. *Trees* 24, 819–832. doi: 10.1007/s00468-010-0452-7

Hu, T. Y., Su, Y. J., Xue, B. L., Liu, J., Zhao, X. Q., Fang, J. Y., et al. (2016). Mapping global forest aboveground biomass with spaceborne LiDAR, optical imagery, and forest inventory data. *Remote Sens*. 8, 565. doi: 10.3390/rs8070565

Hulshof, C. M., Swenson, N. G., and Weiser, M. D. (2015). Tree height-diameter allometry across the United States. *Ecol. E.* 5, 1193–1204. doi: 10.1002/ece3.1328

Jiang, R., Lin, J. Y., and Li, T. X. (2022). Refined aboveground biomass estimation of moso bamboo forest using culm lengths extracted from TLS POINT CLOUD. *Remote Sens*. 14, 5537. doi: 10.3390/rs14215537

Jiang, X. D., Li, G. Y., Lu, D. S., Chen, E. X., and Wei, X. L. (2020). Stratification-based forest aboveground biomass estimation in a subtropical region using airborne lidar data. *Remote Sens*. 12, 1101. doi: 10.3390/rs12071101

Justine, M. F., Yang, W. Q., Wu, F. Z., Tan, B., Khan, M. N., Zhao, Y. Y., et al. (2015). Biomass stock and carbon sequestration in a chronosequence of Pinus massoniana plantations in the upper reaches of the Yangtze River. *Forests* 6, 3665–3682. doi: 10.3390/f6103665

Kuyah, S., Muthuri, C., Jamnadass, R., Mwangi, P., Neufeldt, H., Dietz, J., et al. (2012). Crown area allometries for estimation of aboveground tree biomass in agricultural landscapes of western Kenya. *Agrofor. Syst*. 86, 267–277. doi: 10.1007/s10457-012-9529-1

Lal, R. (2005). Forest soils and carbon sequestration. *For. Ecol. Manage*. 220, 242–258. doi: 10.1016/j.foreco.2005.08.015

Li, F. R. (2019). *Forest Measurement, 4th Edn*. Beijing: China Forestry Publishing House.

Li, L., Guo, Q. H., and Xu, G. C. (2015). Lidar with multi-temporal MODIS provide a means to upscale predictions of forest biomass. *ISPRS-J. Photogramm. Remote Sens*. 102, 198–208. doi: 10.1016/j.isprsjprs.2015.02.007

Li, W. K., Guo, Q. H., Jakubowski, M. K., and Kelly, M. (2012). A new method for segmenting individual trees from the lidar point cloud. *Photogramm. Eng. Remote Sens*. 78, 75–84. doi: 10.14358/PERS.78.1.75

Li, Z. Y., Liu, Q. W., and Pang, Y. (2016). Review on forest parameters inversion using LiDAR. *J. Remote Sens*. 20, 1138–1150. doi: 10.11834/jrs.20165130

Lin, J. Y., Chen, D. C., Wu, W. J., and Liao, X. H. (2022). Estimating aboveground biomass of urban forest trees with dual-source UAV acquired point clouds. *Urban Gree*. 69, 127521. doi: 10.1016/j.ufug.2022.127521

Lin, J. Y., Wang, M. M., Ma, M. G., and Lin, Y. (2018). Aboveground tree biomass estimation of sparse subalpine coniferous forest with UAV oblique photography. *Remote Sens*. 10, 1849. doi: 10.3390/rs10111849

Liu, H. R., Fan, W. W., Xu, Y. S., and Lin, W. S. (2021). Single tree biomass estimation based on UAV LiDAR point cloud. *J. Cent. South Univ. For. Technol*. 41, 92–99.

Liu, K., Shen, X., Cao, L., Wang, G. B., and Cao, F. L. (2018). Estimating forest structural attributes using UAV-LiDAR data in Ginkgo plantations. *ISPRS-J. Photogramm. Remote Sens*. 146, 465–482. doi: 10.1016/j.isprsjprs.2018.11.001

Liu, Z. J., Guan, Y. Y., Xu, Y. L., and Xu, Y. (2019). Analysis on structure feature of Metasequoia glyptostroboides and Ginkgo biloba standing tree in urban area of Qingdao City Guangxi. *For. Sci*. 48, 127–132.

Lu, D. S., Chen, Q., Wang, G. X., Liu, L. J., Li, G. Y., Moran, E., et al. (2014). A survey of remote sensing-based aboveground biomass estimation methods in forest ecosystems. *Int. J. Digit. Earth* 9, 63–105. doi: 10.1080/17538947.2014.990526

Lu, J. B., Wang, H., Qin, S. H., Cao, L., Pu, R. L., Li, G. L., et al. (2020). Estimation of aboveground biomass of Robinia pseudoacacia forest in the Yellow River Delta based on UAV and Backpack LiDAR point clouds. *Int. J. Appl. Earth Obs. Geoinf*. 86, 102014. doi: 10.1016/j.jag.2019.102014

Lu, X. M., Zheng, G., Miller, C., and Alvarado, E. (2017). Combining multi-source remotely sensed data and a process-based model for forest aboveground biomass updating. *Sensors* 17, 2062. doi: 10.3390/s17092062

Lun, F., Liu, Y., He, L., Yang, L., Liu, M. C., Li, W. H., et al. (2018). Life cycle research on the carbon budget of the Larix principis-rupprechtii plantation forest ecosystem in North China. *J. Clean Prod*. 177, 178–186. doi: 10.1016/j.jclepro.2017.12.126

Luo, Y. J., Wang, X. K., Ouyang, Z. Y., Lu, F., Feng, L. G., Tao, J., et al. (2020). A review of biomass equations for China's tree species. *Earth Syst. Sci. Data* 12, 21–40. doi: 10.5194/essd-12-21-2020

Ma, J. S. (2007). A worldwide survey of cultivated Metasequoia glyptostroboides Hu and Cheng (Taxodiaceae: Cupressaceae) from 1947 to 2007. *Bull. Peabody Mus. Natl. Hist*. 48, 235–253. doi: 10.3374/0079-032X(2007)48(235:AWSOCM)2.0.CO;2

Ma, K. S., Chen, Z. X., Fu, L. Y., Tian, W. L., Jiang, F. G., Yi, J., et al. (2022). Performance and sensitivity of individual tree segmentation methods for UAV-LiDAR in multiple forest types. *Remote Sens*. 14, 298. doi: 10.3390/rs14020298

Ming, A. G., Jia, H. Y., Tao, Y., Lu, L. H., Su, J. M., Shi, Z. M., et al. (2012). Biomass and its allocation in a 28-year-old Mytilaria laosensis plantation in southwest Guangxi. *Chin. J. Ecol*. 31, 1050–1056.

Nie, S., Wang, C., Zeng, H. C., Xi, X. H., and Li, G. C. (2017). Above-ground biomass estimation using airborne discrete-return and full-waveform LiDAR data in a coniferous forest. *Ecol. Indic*. 78, 221–228. doi: 10.1016/j.ecolind.2017.02.045

Paul, K. I., Roxburgh, S. H., Chave, J., England, J. R., Zerihun, A., Specht, A., et al. (2016). Testing the generality of above-ground biomass allometry across plant functional types at the continent scale. *Glob. Change Biol*. 22, 2106–2124. doi: 10.1111/gcb.13201

Popescu, S. C. (2007). Estimating biomass of individual pine trees using airborne lidar. *Biomass Bioenerg*. 31, 646–655. doi: 10.1016/j.biombioe.2007.06.022

Popescu, S. C., Wynne, R. H., and Nelson, R. F. (2002). Estimating plot-level tree heights with lidar: local filtering with a crown-height based variable window size. *Comput. Electron. Agric*. 37, 71–95. doi: 10.1016/S0168-1699(02)00121-7

Shi, L., and Liu, S. R. (2017). Methods of estimating forest biomass: a review. *Biomass Vol. Estim. Valoriz. Energ*. 12, 23–46. doi: 10.5772/65733

Su, H. Y., Shen, W. J., Wang, J. R., Ali, A., and Li, M. S. (2020). Machine learning and geostatistical approaches for estimating aboveground biomass in Chinese subtropical forests. *For. Ecosyst*. 7, 64. doi: 10.1186/s40663-020-00276-7

Sun, G., Ranson, K. J., Guo, Z., Zhang, Z., Montesano, P., Kimesb, D., et al. (2011). Forest biomass mapping from lidar and radar synergies. *Remote Sens. Environ*. 115, 2906–2916. doi: 10.1016/j.rse.2011.03.021

Wallace, L., Musk, R., and Lucieer, A. (2014). An assessment of the repeatability of automatic forest inventory metrics derived from UAV-borne laser scanning data. *IEEE Trans. Geosci. Remote Sensing* 52, 7160–7169. doi: 10.1109/TGRS.2014.2308208

Wang, D. Z., Wan, B., Liu, J., Su, Y. J., Guo, Q. H., Qiu, P. H., et al. (2020). Estimating aboveground biomass of the mangrove forests on northeast Hainan Island in China using an upscaling method from field plots, UAV-LiDAR data and Sentinel-2 imagery. *Int. J. Appl. Earth Obs. Geoinf*. 85, 101986. doi: 10.1016/j.jag.2019.101986

Wan-Mohd-Jaafar, W. S., Woodhouse, I. H., Silva, C. A., Omar, H., and Hudak, A. T. (2017). Modelling individual tree aboveground biomass using discrete return lidar in lowland dipterocarp forest of Malaysia. *J. Trop. For. Sci*. 29, 465–484. doi: 10.26525/jtfs2017.29.4.465484

White, J. C., Coops, N. C., Wulder, M. A., Vastaranta, M., Hilker, T., Tompalski, P., et al. (2016). Remote Sens. technologies for enhancing forest inventories: a review. *Can. J. Remote Sens*. 42, 619–641. doi: 10.1080/07038992.2016.1207484

Wu, B., Yu, B. L., Yue, W. H., Shu, S., Tan, W. Q., Hu, C. L., et al. (2013). A voxel-based method for automated identification and morphological parameters estimation of individual street trees from mobile laser scanning data. *Remote Sens*. 5, 584–611. doi: 10.3390/rs5020584

Wu, X., Shen, X., Cao, L., Wang, G., and Cao, F. (2019). Assessment of individual tree detection and crown cover estimation using unmanned aerial vehicle based light detection and ranging (UAV-LiDAR) data in planted forests. *Remote Sens*. 11, 908. doi: 10.3390/rs11080908

Wulder, M., Niemann, K. O., and Goodenough, D. G. (2000). Local maximum filtering for the extraction of tree locations and basal area from high spatial resolution imagery. *Remote Sens. Environ*. 73, 103–114. doi: 10.1016/S0034-4257(00)00101-2

Xu, D. D., Wang, H. B., Xu, W. X., Luan, Z. Q., and Xu, X. (2021). LiDAR applications to estimate forest biomass at individual tree scale: opportunities, challenges and future perspectives. *Forests* 12, 550. doi: 10.3390/f12050550

Yu, Y. F., Song, T. Q., Zeng, F. P., Peng, W. X., Wen, Y. G., Huang, C. B., et al. (2013). Dynamic changes of biomass and its allocation in Cunninghamia lanceolata plantations of different stand ages. *Chin. J. Ecol*. 32, 1660–1666.

Zhao, B. G., Zhu, J., Ai, X. R., Yao, L., Guo, Q. J., Hong, J. F., et al. (2021). Path analysis of DBH and crown width of native Metasequoia glyptostroboides population. *J. Northeast For. Univ*. 49, 16–20.

Zhao, X. Q., Guo, Q. H., Su, Y. J., and Xue, B. L. (2016). Improved progressive TIN densification filtering algorithm for airborne LiDAR data in forested areas. *ISPRS-J. Photogr. Remote Sens*. 117, 79–91. doi: 10.1016/j.isprsjprs.2016.03.016

Zheng, L., Cai, D. X., Lu, L. H., Ming, A. G., Yu, H. L., Li, Z. G., et al. (2014). Biomass allocation of different species plantations in subtropical area of China. *For. Res*. 27, 454–458.